© 2020. Published by The Company of Biologists Ltd | Journal of Experimental Biology (2020) 223, jeb233494. doi:10.1242/jeb.233494

RESEARCH ARTICLE

Structure and function of the nervous system in nectophores of the siphonophore *Nanomia bijuga*

Tigran P. Norekian[1,2,3] and Robert W. Meech[4,*]

ABSTRACT

Although the bell-shaped nectophores of the siphonophore *Nanomia bijuga* are clearly specialized for locomotion, their complex neuroanatomy described here testifies to multiple subsidiary functions. These include secretion, by the extensively innervated 'flask cells' located around the bell margin, and protection, by the numerous nematocytes that line the nectophore's exposed ridges. The main nerve complex consists of a nerve ring at the base of the bell, an adjacent column-shaped matrix plus two associated nerve projections. At the top of the nectophore the upper nerve tract appears to have a sensory role; on the lower surface a second nerve tract provides a motor input connecting the nectophore with the rest of the colony via a cluster of nerve cells at the stem. *N. bijuga* is capable of both forward and backward jet-propelled swimming. During backwards swimming the water jet is redirected by the contraction of the Claus' muscle system, part of the muscular velum that fringes the bell aperture. Contractions can be elicited by electrical stimulation of the nectophore surface, even when both upper and lower nerve tracts have been destroyed. Epithelial impulses elicited there, generate slow potentials and action potentials in the velum musculature. Slow potentials arise at different sites around the bell margin and give rise to action potentials in contracting Claus' muscle fibres. A synaptic rather than an electrotonic model more readily accounts for the time course of the slow potentials. During backward swimming, isometrically contracting muscle fibres in the endoderm provide the Claus' fibres with an immobile base.

KEY WORDS: Anti-tubulin antibody, Epithelial conduction, Intracellular recording, Nervous system, Swimming behaviour, Unstriated muscle fibres

INTRODUCTION

The most striking feature of the behaviour of the siphonophore *Nanomia* is that it is able to take evasive action by rapidly swimming either backwards or forwards. In either case, movement depends on the contraction of bell-like structures, the nectophores, that form a column at the anterior end of the colony (Fig. 1A). Each nectophore resembles a medusa 'stripped of its gonads, tentacles, mouth and manubrium' (Mackie et al., 1987). Its ring-shaped nervous system receives an input from the rest of the colony via nerves in the stem-like structure that links the different parts of the colony together. As with other hydromedusan swimming bells, the thrust for movement originates in the contraction of a striated muscle sheet, the myoepithelium, lining the subumbrella cavity of the bell. Under normal conditions water is forced out of the bell and the animal is jet-propelled forward. Mackie (1964) has shown that backward swimming depends on the contraction of specialized radial muscles. These are Claus' fibres, part of a thin muscular diaphragm (velum) that runs around the bell aperture. When Claus' fibres contract, the water expelled from the bell is redirected forwards.

Given the apparent simplicity of the nectophore nerve circuits, the challenge was to explain the way in which its different muscle groups are controlled. Mackie (1964) found that for forward swimming, signals pass from the stem to the subumbrella musculature via a specific route, the lower nerve tract. In contrast, stimuli that evoke reverse swimming follow no single localized route and are carried all over the outer surface of the nectophore, by way of a non-muscular excitable epithelium. The way in which excitation passes from the excitable epithelium to the Claus' fibres was unclear. There was no evidence for chemical synapses between epithelium and muscle and it seemed possible that the link depended on electrical junctions instead.

This paper presents the neuroanatomy of the nectophore, and shows that although *Nanomia* nectophores are clearly specialized for locomotion, their different cellular elements and nerve structures testify to the existence of subsidiary functions. Intracellular recordings from Claus' fibres show that the action potentials associated with muscle contraction arise from slower, depolarizing events originating at sites around the margin of the bell. The balance of evidence is such that these slow potentials probably represent a synaptic input from ring nerves in the bell margin.

MATERIALS AND METHODS

Animals

Adult specimens of *Nanomia bijuga* (Delle Chiaje 1844) were collected from surface water at the dock of the Friday Harbor Laboratories, University of Washington, USA, and held in 2 l jars of seawater at 7–9°C. Animals survive in good condition for several days but wherever possible electrophysiology experiments were carried out on freshly collected specimens. We used the largest, older nectophores from a colony so as to maximize the accuracy of length measurements. Mackie (1964) reports that in intact colonies, electrical stimulation of younger, anterior nectophores produced reverse swims but when older nectophores were used, swims were directed forward. We have found that once isolated, even the oldest nectophores exhibit Claus' fibre contractions and fictive reverse swims, suggesting that it is transmission to the rest of the colony that fails in the older nectophores. We found no anatomical differences between nectophores from anterior or posterior regions. Experiments were performed in the spring–summer seasons of 2016–2020.

Terminology

Haddock et al. (2005) provide a comprehensive terminology to specify the axes of siphonophores. We follow them in using the term

[1]Whitney Laboratory for Marine Biosciences, University of Florida, St Augustine, FL 32080, USA. [2]Friday Harbor Laboratories, University of Washington, Friday Harbor, WA 98250, USA. [3]Institute of Higher Nervous Activity and Neurophysiology, Moscow 117485, Russia. [4]School of Physiology, Pharmacology and Neuroscience, University of Bristol, Bristol BS8 1TD, UK.

*Author for correspondence (r.meech@bristol.ac.uk)

T.P.N., 0000-0002-7022-1381; R.W.M., 0000-0003-0199-9066

Received 18 July 2020; Accepted 29 October 2020

Journal of Experimental Biology (2020) 223, jeb233494. doi:10.1242/jeb.233494

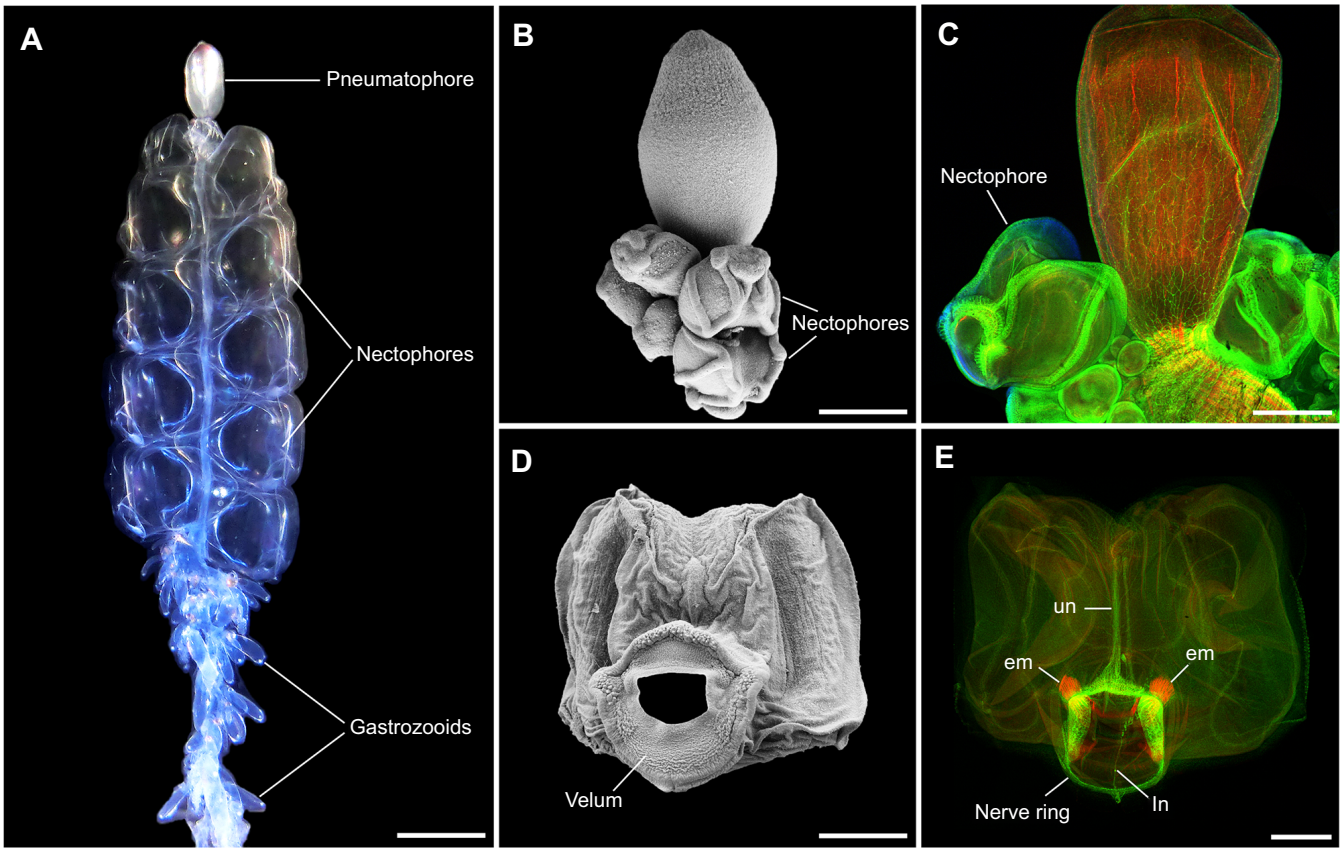

Fig. 1. General view of the nectophores of *Nanomia bijuga*. (A) Anterior region of the colony showing pneumatophore, nectophores and gastrozoids. The stem is visible through the transparent nectophores. (B,C) Scanning electron microscopy (SEM) image (B) and anti-tubulin antibody/phalloidin-stained image (C) of a neumatophore with young nectophores attached at its base. (D,E) SEM image (D) and anti-tubulin antibody/phalloidin-stained image (E) of a nectophore. Anti-tubulin antibody, which labels the neural system, is green, while phalloidin, which labels F-actin is red. em, endodermal muscle fibres; ln, lower nerve tract; un, upper nerve tract. Scale bars: A, 5 mm; B–E, 500 µm.

'anterior' to describe the end of the colony with the pneumatophore. We also use the terms 'upper' and 'lower' to replace the terms 'dorsal' and 'ventral' in isolated nectophores, 'dorsal' and 'ventral' being retained as descriptors for the entire colony. For the experimental work on isolated nectophores, we have found it convenient to use the terms 'distal' and 'proximal' to the margin to describe muscle locations.

Scanning electron microscopy (SEM)

Nectophores were detached from adult *N. bijuga* and fixed in 2.5% glutaraldehyde in 0.1 mol l^{-1} phosphate-buffered saline (PBS; pH 7.6) for 3–5 h at room temperature. They were then washed for several hours in 2.5% sodium bicarbonate. For secondary fixation, the samples were incubated in 2% osmium tetroxide, 1.25% sodium bicarbonate for 3 h at room temperature. They were rinsed several times with distilled water, dehydrated in ethanol (10 min each in 30%, 50%, 70%, 90% and 100% ethanol) and then placed in 100% ethanol in a Samdri-790 unit (Tousimis Research Corporation) for critical point drying. The nectophore has a relatively thin body wall and so the intermediate fluid, ethanol, could be replaced with liquid CO_2 using only 4–5 short purging cycles, with time between cycles to allow for good penetration. The protocol was established manually and based on experimental outcomes. After the drying process, the samples were mounted on holding platforms and processed for metal coating using an SPI Sputter Coater with a gold/palladium target. To ensure an even coating, the sample was coated twice, the platform being rotated 180 deg between coatings. SEM imaging was performed using a NeoScope JCM-5000 microscope (JEOL Ltd, Tokyo, Japan).

Immunocytochemistry

Detached *N. bijuga* nectophores were fixed overnight in 4% paraformaldehyde in 0.1 mol l^{-1} PBS (5°C; pH 7.6) and then washed for 2 h in PBS. This and all subsequent incubations took place under refrigeration at 5°C. The specimens were pre-incubated for about 6 h in a blocking solution of 6% goat serum in PBS, and then incubated for a further 48 h in the primary anti-tubulin antibody diluted in blocking solution at a final dilution of 1:40. The rat monoclonal anti-tubulin antibody (AbD Serotec, Bio-Rad, MCA77G, RRID: AB_325003) recognizes the alpha subunit of tubulin, and specifically binds tyrosylated tubulin (Wehland and Willingham, 1983; Wehland et al., 1983). Following a series of PBS washes for 6–8 h, the specimens were incubated for 24 h in secondary goat anti-rat IgG antibodies (Alexa Fluor 488 conjugated; Molecular Probes, Invitrogen, WA, MA, A11006, RRID: AB_141373) at a final dilution 1:20. To label the muscle fibres, we used the well-known marker phalloidin (Alexa Fluor 568 phalloidin from Molecular Probes, Invitrogen, A11077, RRID: AB_2534121), which binds to F-actin. Following secondary antibody treatment, the specimens were incubated in phalloidin solution (in 0.1 mol l^{-1} PBS) for 8 h at a final dilution 1:80 and then washed for 6–8 h in several PBS rinses.

To stain the nuclei, the preparations were mounted in mounting medium with DAPI (Vectashield) on glass microscope slides. The slides were viewed and photographed using a Nikon Research Microscope Eclipse E800 with epi-fluorescence using standard TRITC and FITC filters and a Nikon C1 laser scanning confocal microscope. To test for the specificity of immunostaining, either the primary or the secondary antibody was omitted from the procedure. In either case, no labelling was detected. This anti-tubulin antibody has been used to label the neural systems in the hydrozoan *Aglantha digitale* (Norekian and Moroz, 2020b) and several ctenophore species (Norekian and Moroz, 2016, 2019a, 2019b, 2020a).

Intracellular recording

Isolated nectophores stabilized with cactus (*Opuntia*) spines in a transparent Sylgard-coated dish were bathed in seawater at 10–15°C. They were illuminated from below and 10% isotonic $MgCl_2$ was used to suppress contractions of striated muscle (see Kerfoot et al., 1985). A bipolar stainless-steel stimulating electrode placed on the exumbrella epithelium provided a 1–2 ms stimulating pulse, which was adjusted to be just suprathreshold in order to minimize local damage. Contractile responses identified the Claus' fibre region of the velum. Micropipettes filled with 3 mol l^{-1} KCl (resistance 40–50 MΩ) were used to monitor the intracellular response at different sites in the velum. Cnidarian muscle units such as the Claus' fibre region consist of electrically coupled sheets of myoepithelial cells. The Claus' fibre region is about 200 µm wide and 300 µm long, with individual muscle 'fibres' being 3–5 µm in diameter. Despite its relatively small size, penetration of the sheet is surprisingly easy and we suppose that the micropipette becomes lodged in the epithelial cell body, which in myoepithelial cells is connected to the contractile component by a short 'neck'. The electrical properties of this essentially two-dimensional system have been explored experimentally in other Hydrozoa (Josephson and Schwab, 1979; Kerfoot et al., 1985) and found to match the theoretical basis provided by Jack et al. (1975). Here, penetration of the sheet was accomplished by briefly overcompensating the negative capacitance adjustment on a World Precision Instruments Model KS700 preamplifier. Individual variation in the dimensions of different nectophores meant that it was necessary to describe the location of the micropipette in general terms. Some Claus' fibre penetrations were sufficiently long lasting for stimulations to be repeated multiple times, but often the micropipette was dislodged by the associated muscle contraction. In non-contracting areas, penetrations lasted many minutes. To identify these different sites, the location of the stimulating electrode and the position of each micropipette were recorded photographically.

Jack et al. (1975) have provided a theoretical account of current flow in a thin sheet of electrically coupled cells. They suggest that current density decreases with distance from a source partly through current flow across intervening cell membranes but also because the increase in intracellular volume with distance has a 'dilution' effect. These two actions mean that the voltage response to a short current pulse decays rapidly. It depends on the membrane time constant (τ_m) and the two-dimensional space constant (λ_2). The value for λ_2 found in an epithelial sheet was 1.3 mm (*Euphysa japonica*; Josephson and Schwab, 1979), while in a myoepithelium (measured along the muscle fibre axis) it was 0.77 mm (*Aglantha digitale*; Kerfoot et al., 1985). In *Aglantha*, τ_m was found to be 5–10 ms and assuming a similar value for the Claus' fibres, we would expect an electrotonic transient recorded within 0.25 mm of the margin to decay to e^{-1} of its peak value in less than 1 ms.

Extracellular recording

As with intracellular recording, the locations of the stimulating electrode and the recording pipette were stored photographically but the recordings were made with a low-resistance extracellular glass suction pipette (tip diameter, 10–15 µm) rather than a high-resistance intracellular one. The pipette was made from glass haematocrit tubes using a two-step pull. Suction was maintained on the velar surface using an air pump connected to the pipette housing so that contact was retained despite the movement of the Claus' fibres. Currents were recorded using a custom-made 'loose patch' clamp amplifier (Roberts and Almers, 1992). The amplitude of the externally recorded current depended on the size of the pipette tip, the area of membrane drawn into the pipette and the amount of current that flows to ground along the surface of the glass.

Video analysis of velum movements

To examine the time course of the Claus' fibre contraction, video sequences (30 frames s^{-1}) were analysed frame by frame. Transects of the contractile region (3 pixels wide) were examined and the change in transmitted light intensity was plotted pixel by pixel before and after stimulation of the exumbrella epithelium. To provide a baseline, the transmitted light intensity was recorded over a 500 ms period (i.e. 15 frames) with the nectophore at rest, and the average pixel intensity calculated for each point. These baseline values were subtracted from intensity data derived from subsequent video frames. Any increase in pixel intensity at the edge of the velum is a direct consequence of the contraction, the velum no longer being in the light path. Away from the edge, changes in pixel intensity represent changes in the path length; formation of a ridge, or fold, would increase path length and reduce pixel intensity; local stretching would decrease path length and increase pixel intensity. Pixel intensity might also be affected by changes in refraction. The aim of the method was limited to identifying regions of the velum that undergo lateral movement. In some experiments, movement in specific areas was monitored by estimating changes in the average pixel intensity at that site.

RESULTS

General structure

In essence, *N. bijuga* consists of a float (pneumatophore) and an extended trailing stem, which runs through the colony's entire length and serves as an anchor for numerous specialized zooids. Attached to the stem, just under the float, are the medusa-like swimming bells (nectophores). Below the nectophores are the gastrozooids, specialized for digestion and with tentacles to trap prey. Also present are transparent bracts, which are thought to contribute to floatation (Jacobs, 1962). Fig. 1A is a photograph of the nectophore region showing its relationship to the rest of the colony. Newly developing nectophores arise just below the pneumatophore and an SEM image of the region shows several at an early stage of development (Fig. 1B), three of them with distinct rounded ridges. Even young nectophores contribute to swimming (Costello et al., 2015) and all resemble small medusae, each with a velar opening facing outwards. The bell undergoes partial collapse during fixation and dehydration, but under SEM the ridge structure is still evident, as is the broad velum (Fig. 1D).

In Fig. 1C, the pneumatophore is stained with a marker for F-actin (phalloidin; red) and an anti-tubulin antibody (green) which binds to microtubule inter-repeat regions, present in large numbers in much nervous tissue. The entire surface of the pneumatophore appears to be covered by a network of anti-tubulin antibody labeled fine nerves, supporting the view that it has an important sensory

Journal of Experimental Biology (2020) 223, jeb233494. doi:10.1242/jeb.233494

function (Church et al., 2015). In Fig. 1E, the nectophore is orientated to match that in Fig. 1D and the anti-tubulin staining shows the main nerves; the upper nerve tract, the lower nerve tract and the nerve ring. Phalloidin staining reveals the position of an important endodermal muscle. Fig. S1 shows a schematic representation of a cross-section through the nectophore.

Two sets of muscle fibres are of particular importance for the current investigation. They are Claus' fibres, located symmetrically on the upper right and upper left of the velum aperture, and the pair of endodermal fibres that abut them. These muscle groups are brought into play during backward swimming. In Fig. 2A, the arrows indicate the position of Claus' fibres. Fixation has caused them to contract and the image approximates to the form that the velum takes during backward swimming. In Fig. 2B (same orientation as Fig. 2A), the Claus' fibres are revealed by phalloidin staining (red). Phalloidin also stains other velar muscles as well as the endodermal muscles. The nerve ring (green) encircles the nectophore at the edge of the velum. It consists of an 'inner' and an 'outer' ring divided by a 0.5 µm thick mesogloea (Jha and Mackie, 1967) but the separation is not visible at this magnification. The upper nerve tract enters the nerve ring at the top of the figure, while the lower nerve tract, which arises from the back of the nectophore, enters at the bottom.

Lower nerve tract

The lower nerve tract, which travels in the ectoderm and enters the nerve ring from the under-surface of the nectophore, can be traced backwards to the point of contact between the nectophore and the stem. The whole pathway is shown in Fig. 2B, although, because the nectophore has been compressed slightly for the purposes of photography, its passage is 'kinked' by a fold in the nectophore wall. At the back of each isolated nectophore there is a narrow scar, visible with both SEM (arrows in Fig. 2C) and confocal microscopy (Fig. 2D). This we take to be the point of separation between the nectophore and stem (autotomy point). The lower nerve runs to the centre of the scar and ends in a group of closely attached, anti-tubulin antibody-stained cells. This 'terminal group' (Fig. 2D) consists of 40–50 tightly packed cells, each about 6–8 µm in diameter and each with a single large nucleus (Fig. 2E). The lower nerve tract arises from within the terminal group and does not branch until it arrives at the nerve ring. Its function is to initiate forward swimming by carrying impulses from the stem (Mackie, 1964).

Upper nerve tract

In contrast to the lower nerve tract, the upper nerve tract is highly branched and covers a large area of the top and back surfaces of the nectophore. It connects to the nerve ring with a wide delta-shaped base (Fig. 3A). On either side of the delta, running parallel to the main tract, many short neurites merge with the nerve ring (arrows in Fig. 3A). These short neurites extend outwards to the exumbrella epithelium. The delta area itself is a complex structure containing numerous nuclei and resembles a ganglion more than a simple collection of nerve fibres (Fig. 3B). Although regions in the delta area and main tract sometimes show phalloidin staining (see also Grimmelikhuijzen et al., 1986), the presence of co-localized anti-tubulin antibody labelling argues against their being muscle units and we take them to be neurites with unusually high levels of F-actin.

Beyond the delta area, at the top of each nectophore, the upper tract is joined by numerous thin lateral neurites (Fig. 3C). At its distal end, the tract breaks up into a mass of fine neurites that cover the entire back surface of the nectophore (Fig. 3G). Most branches end in neural cell bodies, each having a single DAPI-stained nucleus (Fig. 3C,D). The cell bodies are found at dispersed locations and are slightly elongated spheres 8–10 µm in diameter (Fig. 3E,F). They

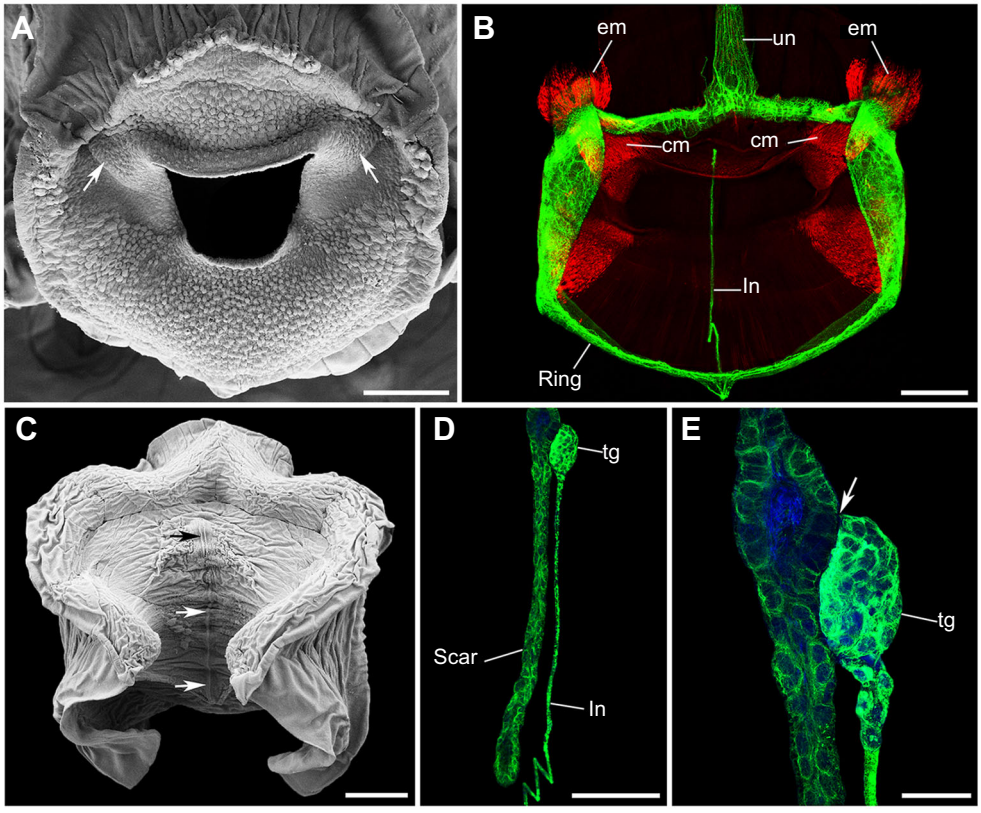

Fig. 2. Nectophore structure and innervation. (A) SEM image of the velum; arrows show the location of Claus' muscle fibres. (B) Nerve elements labelled with anti-tubulin antibody (green); F-actin in muscles labelled with phalloidin (red). (C) SEM image of the nectophore from the back; arrows show the connection to the stem (scar). (D) Lower nerve tract labelled with anti-tubulin antibody (green); this ends in a 'terminal group' of cells attached to the centre of the scar. (E) Point of attachment (arrow) between the 'terminal group' and the epithelial scar. cm, Claus' muscle fibres; em, endodermal muscles; In, lower nerve tract; Ring, nerve ring; tg, terminal group; un, upper nerve tract. Scale bars: A and B, 200 µm; C, 400 µm; D, 150 µm; E, 40 µm.

Journal of Experimental Biology (2020) 223, jeb233494. doi:10.1242/jeb.233494

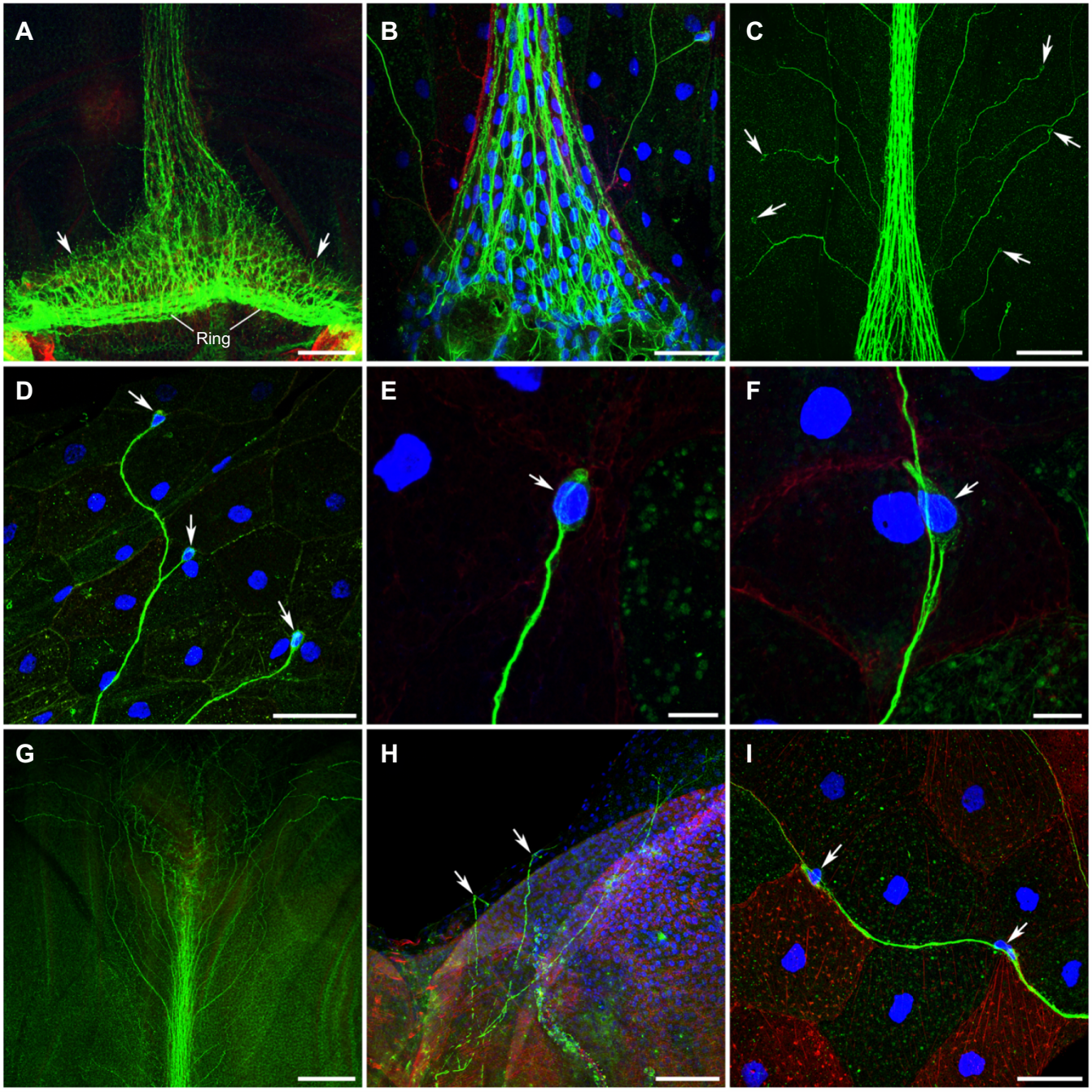

Fig. 3. Upper nerve tract stained with anti-tubulin (green), phalloidin (red) and DAPI (blue). (A) The delta region at the base of the upper nerve tract where it connects to the nerve ring (Ring). Note the many short neurites that join the nerve ring (arrows). (B) Delta region at higher magnification showing numerous nucleated cells. Note phalloidin labelling within the tract itself. (C) Upper nerve tract near its base showing dispersed branches and oval cell bodies (arrows). (D) Cell bodies (arrows) of unipolar neurons whose branches travel together towards the main trunk of the upper nerve. (E) Neural cell body at higher magnification with a large DAPI-stained nucleus (arrow). (F) Unipolar neuron (arrow) alongside a nerve branch travelling towards the upper nerve tract. (G) Branches of the upper nerve tract that cover the back of the nectophore. (H) Nerve branches in the epithelial layer of the exumbrella (arrows); the phalloidin-stained striated muscle layer in the subumbrella is visible through the mesogloea. (I) A nerve branch navigating its way between large epithelial cells outlined by phalloidin and anti-tubulin antibody staining (4 µm thick section). Arrows show neural cell bodies. Scale bars: A, 100 µm; B, 40 µm; C, 200 µm; D, 50 µm; E and F, 10 µm; G, 200 µm; H, 100 µm; I, 40 µm.

are also located mid-way along neural fibres (Fig. 3F,I) and their processes add to the common neural thread (Fig. 3F). We suggest that these cells are sensory in nature, gathering information from all over the back of the nectophore, their processes joining to form thicker and thicker nerves until they reach the main upper nerve tract. In much the same way a river collects water from numerous small streams, information apparently flows from the periphery to the nerve ring by way of the main upper nerve tract.

All branches of the upper nerve tract run in the exumbrella epithelium (Fig. 3H), navigating their way between the epithelial

Journal of Experimental Biology (2020) 223, jeb233494. doi:10.1242/jeb.233494

cells. Fig. 3I shows a thin branch of the upper nerve tract running precisely between the epithelial cells, clearly outlined by phalloidin and anti-tubulin antibody staining (optical section less than 4 µm thick).

Nerve ring

In common with other hydrozoan swimming bells (Satterlie and Spencer, 1983), *N. bijuga* nectophores have a nerve ring at the edge of the velum, which acts as a command centre responsible for swimming (Fig. 2B). Fig. 4A shows the nerve ring as it crosses the junction between the Claus' fibres and the endodermal muscle group. In optical serial sections, the nerve ring can be seen to deviate in its course towards this more deeply located junction. Fig. 4C, which is from a different preparation to Fig. 4A and is at a different angle, reveals the bend of the ring nerve as it dives toward the muscle junction (see arrow).

The nerve ring is not the only nerve complex present in the nectophore. Fig. 4 shows that near the Claus' fibre region, and connected with the nerve ring, is a dense network of neural cell bodies and fibres that form a wide somewhat cylindrical structure. Two of these lateral networks, located symmetrically on either side of the velum, appear to lie beneath a region containing light-sensitive chromatophores (Mackie, 1962). Each lateral network acts as a base for two projections of neural fibres that extend on either side. One, the 'z' projection, is shorter and directed outwards towards the bell surface (Fig. 4A). It appears to innervate the 'seitliche Zapfen' (Claus, 1878) – an epithelial thickening that acts as a landmark on either side of the exumbrella. The second projection is a cone-shaped fringe of long nerve processes, extending towards the velum and Claus' muscle group (Fig. 4A,B, arrowheads).

In each of the upper corners of the velum next to the lateral network are groups of flask-shaped structures that stain with anti-tubulin antibody (Fig. 5A,B). Similar rounded cells are found in another densely innervated area at the base of the upper nerve tract where it joins the nerve ring (Fig. 5A). SEM imaging suggests that these cells are secretory in nature (Fig. 5C,D). In Fig. 5B,D (arrows), many of them appear to have released their contents, making their openings evident.

Nematocytes

Nanomia bijuga nectophores have a distinctive pattern of exumbrellar ridges and depressions that reflect the way they pack together along the stem. These ridges, particularly the two on the upper surface that face the outside, are populated by rows of nematocytes. that stain positive with anti-tubulin antibody (Fig. 6A-C).They are seen as cone-shaped cells with a single short cilium (arrows in Fig. 6C,D) and a single large nucleus (Fig. 6D,E). At the base of each cilium is a narrow ring that stains with phalloidin (Fig. 6C–E). Branches of the upper nerve tract frequently cross or run along the ridges (Fig. 6D), and sometimes overlap with individual nematocytes (Fig. 6E).

In many SEM images, nectophore ridges exhibit rows of hair-like structures, 70–80 µm in length and 1.5 µm thick, which we take to be tubules of discharged nematocysts (Fig. 6F,G) triggered by the glutaraldehyde fixation process. Untriggered nematocysts can be identified by a short sensory cilium – the cnidocil (Fig. 6G). At higher magnification, the discharged tubules are seen to consist of several helical filaments tightly twisted together (Fig. 6G); three filaments have serrated edges. The tubules are non-tapering, with square ends and are closed at the tip. They correspond to the astomocnidae class of nematocyst (Weill, 1934), appear to be non-penetrating and are thought to entangle their targets (Mariscal, 1974; Östman, 2000).

Muscle structure

The redirection of the swimming thrust in *N. bijuga* is achieved through the contraction of two symmetrical sets of paired radial smooth muscles. Each pair consists of Claus' fibres in the velum abutting a second muscle group in the endoderm (Fig. 2B), their combined action representing a truly remarkable specialization. At high magnification, the junction between the two sets of fibres shows a clear separation (Fig. 7A), with the ends of endodermal fibres being attached to what appears to be a basement membrane (Fig. 7C, arrows). Each group of Claus' fibres is about 200 µm wide and 300 µm long, with individual muscle 'tails' being 3–5 µm thick. Claus' fibres are myoepithelial cells, like other cnidarian muscles, and their epithelial cell bodies line the outer surface of the velum. The distal ends of the endodermal muscle fibres are in contact with

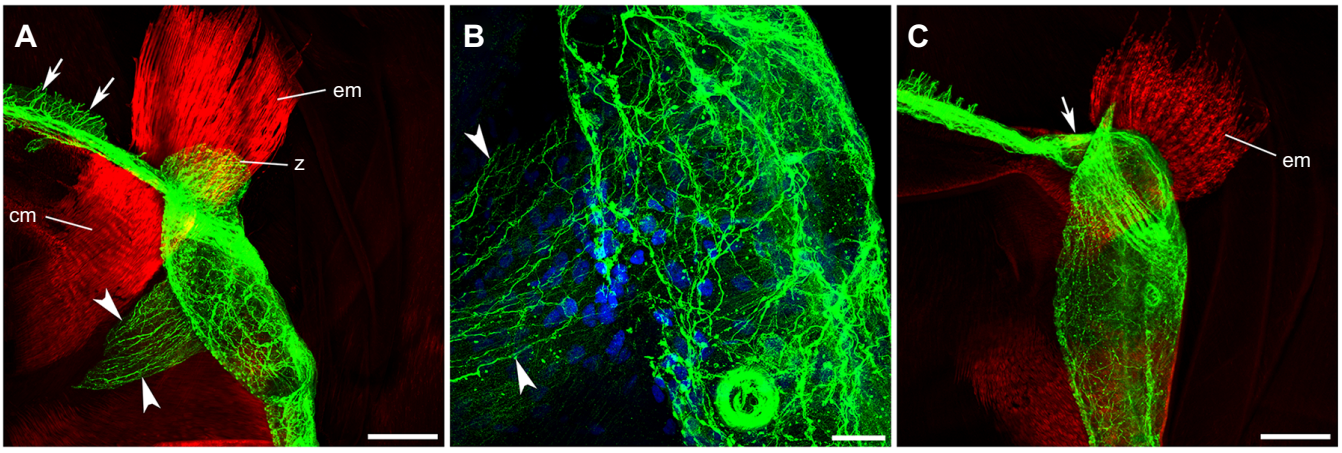

Fig. 4. Nerve ring and associated neural network. (A) Nerve ring crossing the junction between Claus' muscle fibres (cm) and endodermal muscle fibres (em). A dense network of neural fibres and cell bodies is attached to the nerve ring on its lateral side next to the Claus' muscle group. Two projections of neural fibres extend from each network. One projection (z) extends toward the 'seitliche Zapfen' area (Claus, 1878) in the epithelium. The second is a cone of neural fibres (arrowheads) projecting into the velum toward the Claus' fibres. Arrows show the short neural processes on the upper side of the nerve ring next to the upper nerve tract, which extend to the epithelial layer. (B) The dense neural network at high magnification. Arrowheads show the cone-shaped projection. Different preparation from that in A. (C) As for A but from a different angle showing how the ring nerve bends and dives toward the junction between Claus' fibres and endodermal muscles (arrow). Scale bars: A and C, 100 µm; B, 25 µm.

Journal of Experimental Biology (2020) 223, jeb233494. doi:10.1242/jeb.233494

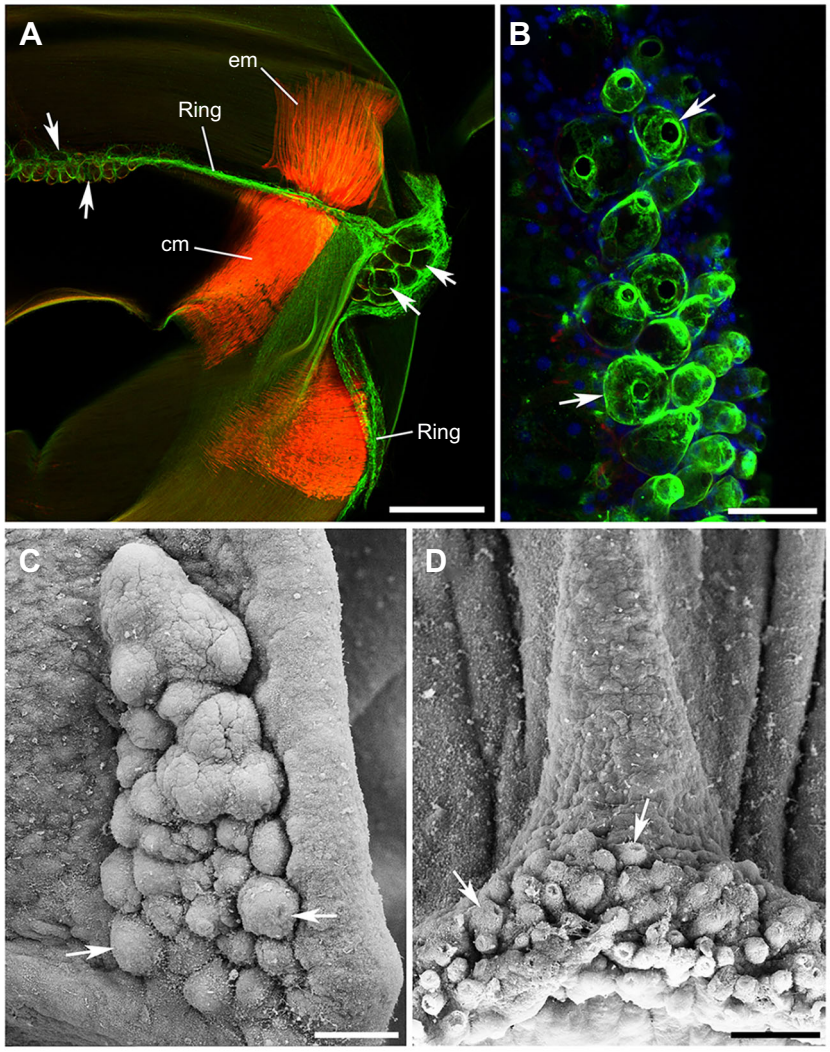

Fig. 5. Secretory cells in the nectophore velum. (A) Anti-tubulin antibody (green) labels two groups of secretory cells located along the nerve ring (Ring). One, central, group is at the base of the upper nerve tract (arrows at left). The second, lateral, group is exactly above the symmetrical nerve networks on either side of the velum (arrows at right), where Claus' muscle fibres (cm) meet the endodermal muscle (em). (B) Higher magnification image of lateral secretory cells labelled by anti-tubulin antibody. DAPI staining shows epithelial cell nuclei. (C) SEM image of lateral secretory cells. (D) SEM image of central secretory cells. Scale bars: A, 200 µm; B–D, 50 µm.

the endodermal lamella (Fig. 7B), an epithelial layer attached to the thin mesogloea that lies above the swim muscles of the subumbrella. This circular muscle layer is about 10 µm thick (fibre diameter 2 µm) and shows clear striations with phalloidin labelling (Fig. 7D).

In addition to the Claus' fibres, the velum also has other, less well-developed radial smooth muscle fibres on its exumbrella surface. The subumbrella surface is entirely covered by circular muscle fibres, which are striated under high magnification. In other hydromedusae, these two muscle groups control the shape of the velum during swimming (Gladfelter, 1972; Fig. 7E).

Claus' fibre movements

Photographic images collected at 30 frames s^{-1} show that stimulation of the exumbrella produces a relatively small change in the velum. Fig. 8A shows a typical example selected from 15 sets of images taken from three different nectophores. The main effect is a slight widening at the upper edge of the velum aperture. Other velum muscles remain relaxed so that contraction of the Claus' fibres is just sufficient to deflect the expelled water onto the concave surface formed by the ballooning of the velum's lower half (see fig. 4C in Mackie, 1964).

Claus' fibres are restricted to a narrow strip on either side of the upper velum but their contraction (arrows in Fig. 8Aii) stretches the entire mid-region (below the delta area), producing a marked fold just within the velum's distal edge (stars in Fig. 8Aiii). To examine the time course of the Claus' fibre contraction, video sequences were analysed frame by frame as described in Materials and Methods. Fig. 8B shows changes in transmitted light in a typical transect crossing a contractile region. The figure consists of seven frames collected before the stimulus (dark blue traces; 67 ms interval), three frames following the stimulus (light blue traces; 67 ms intervals) and 13 frames collected during recovery (purple traces; five at 67 ms intervals then eight at intervals of 334 ms). It is evident that there is little change in the light path in the region above the endodermal muscle and that movement is largely confined to the velum. At the velum's distal edge, there is a large increase in pixel intensity as it retracts from the light path. At the point indicated by the blue filled circle in Fig. 8B, the pixel intensity is reduced, the point of maximum reduction corresponding to a fold at the edge of the velum. Over the course of the video sequence, the pixel intensity slowly returns to its resting level with the abrupt transition in light intensity at the distal rim of the velum gradually subsiding. As this occurs, the point of maximum reduction in transmitted light, i.e. the fold, moves in the distal direction (shown by the open arrow in Fig. 8B).

Not all the intensity changes in Fig. 8B arise from radial displacement of the distal velum. In other regions, the peaks and troughs of the pixel intensity change do not greatly alter their position. This suggests that the movement of the distal velum pushes

Journal of Experimental Biology (2020) 223, jeb233494. doi:10.1242/jeb.233494

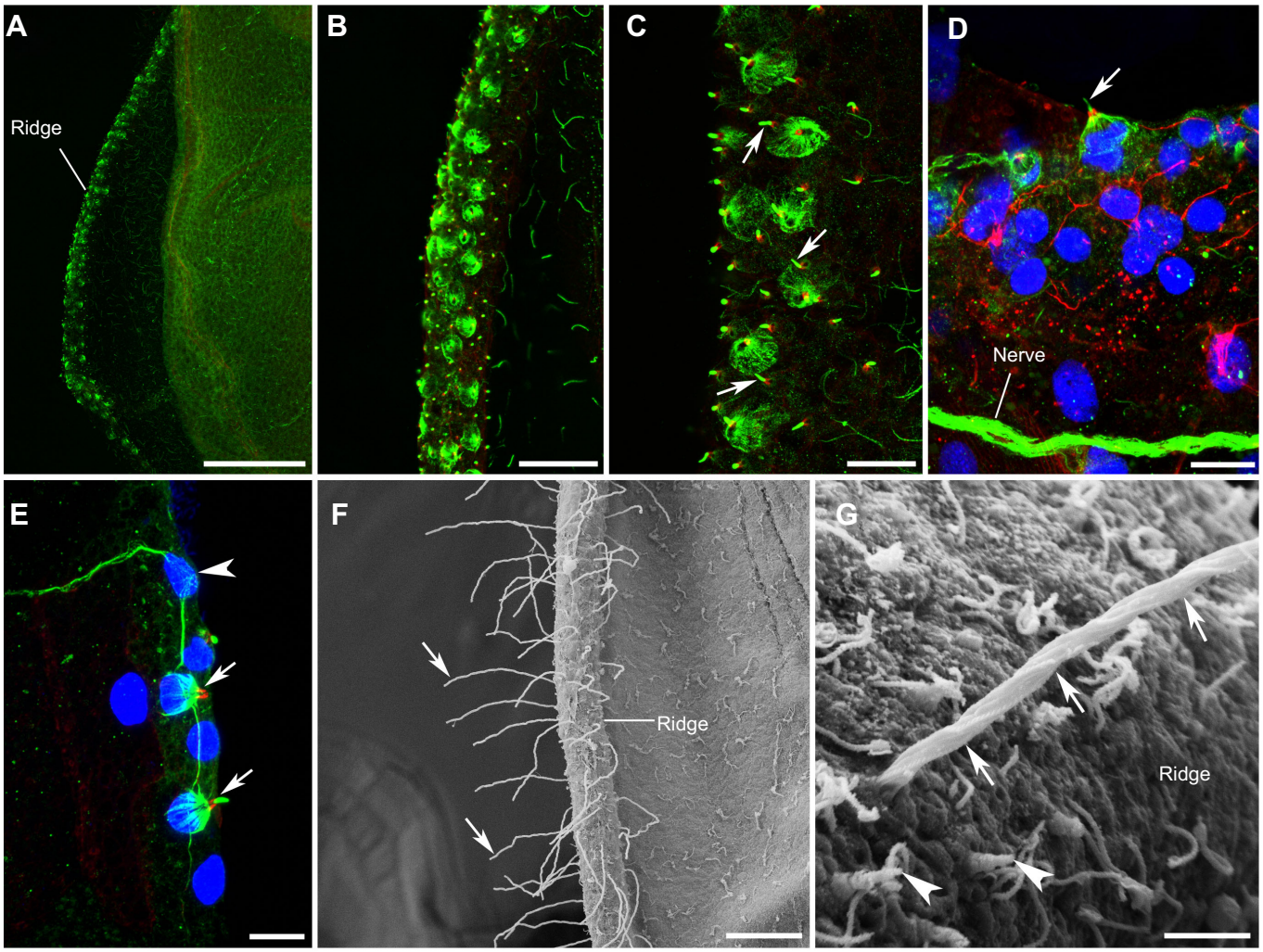

Fig. 6. Nematocytes in nectophore ridges stained with anti-tubulin antibody (green), phalloidin (red) and DAPI (blue). (A,B) Nectophore ridges with numerous cone-shaped nematocytes. (C) Nematocysts with a single short cilium (cnidocil; arrows). (D) Each cilium (arrow) has a phalloidin-labeled base; phalloidin has also outlined the epithelial cells. (E) Fine neural process overlapping two nematocytes (arrows). Arrowhead shows bipolar neural cell body, which sends a process to the upper nerve tract. (F) SEM image showing hair-like structures along the nectophore ridges (arrows). (G) At higher magnification, it can be seen that the hairs consist of individual filaments tightly twisted together (arrows). The tubule is undifferentiated along its length and has three rows of serrations projecting about 0.25 μm. Arrowheads show short protruding cilia, which may be the cnidocils of undischarged nematocytes. Scale bars: A, 200 μm; B, F, 50 μm; C,D, 25 μm; E, 10 μm; G, 5 μm.

more proximal regions into corrugations. These folds appear immediately after the stimulus and then subside during the course of recovery. Apart from the region in the vicinity of the nerve ring (yellow dashed line at 0 mm in Fig. 8B), there is little intensity change of any kind outside the velum. This includes the region overlying the endodermal muscle fibres.

Fig. 8C shows the effect of repeated stimuli on different positions in and around the velum. There are marked changes in average transmitted light in Claus' fibre areas, but minimal change at other sites. This is true not only in the lateral areas but also in the region at the top of the velum immediately under the delta region. More distally in this mid-region, small changes are evident caused by contractions in neighbouring Claus' fibres. The nature of the intensity change depends on the position of the selected area. At the distal edge of the velum, movement is seen as an increase in average pixel intensity; at more proximal positions, the change will depend on whether or not the selected region was located on a natural fold.

In these experiments, the stimulating electrode was positioned on the far left-hand side of the nectophore and the responses from the nearer Claus' fibres were stronger than from those on the right. A cut in the sub-delta region of the velum enhanced the Claus' fibre movements, suggesting that the velum is normally held in tension and a small delay could produce an imbalance between the two sides. The cut also caused movements in the area above the endodermal muscle fibres. We suppose that the conformation of the velum during backwards swimming depends on a delicate balance between Claus' fibre contractions on either side, the endodermal muscle contractions and the tension in the sub-delta region.

Electrophysiology

The effect of stimulating the exumbrella on the Claus' fibre system was examined using intracellular micropipettes. Fig. 9A shows a schematic representation of the velum, traced from stored images, for five nectophore preparations. In the figure, the velum is yellow with darker areas representing the approximate limits to the visible

Journal of Experimental Biology (2020) 223, jeb233494. doi:10.1242/jeb.233494

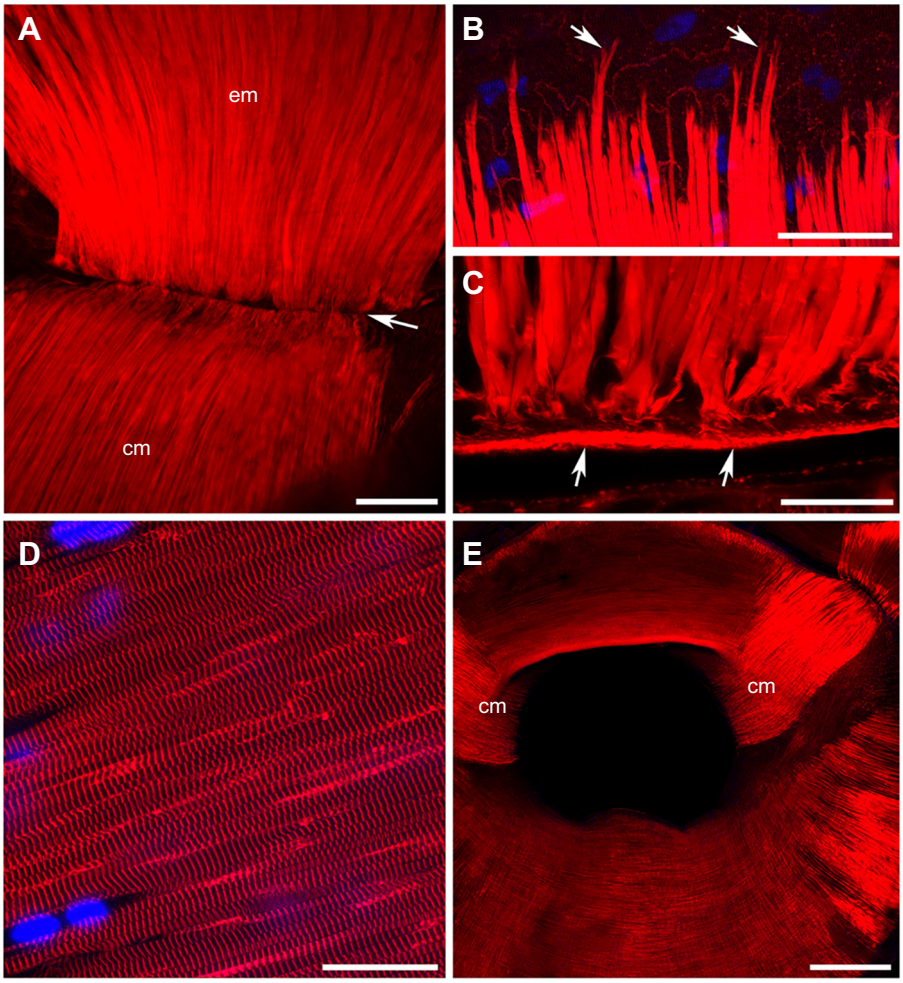

Fig. 7. Nectophore muscles labelled with phalloidin. (A) Junction (arrow) between Claus' muscle fibres (cm) and the endodermal muscle fibre group (em). (B) Distal ends (arrows) of endodermal muscle fibres terminate in an endodermal epithelium attached to the mesogloea. (C) Proximal ends of endodermal muscle fibres attached to a basement membrane (arrows) at the point of contact with Claus' muscle group. (D) Striated circular muscle fibres in the subumbrella ectoderm. (E) Smooth radial muscle fibres on the exumbrella surface and striated circular muscle fibres on the subumbrella surface of the velum. Scale bars: A, 50 µm; B–D, 25 µm; E, 200 µm.

contractions. The records in Fig. 9B–E show the three main kinds of intracellular response to epithelial stimulation. For each pair of records, the recording location of the thicker trace is indicated on the chart (Fig. 9A), the thinner trace being recorded from a neighbouring site. In 15 sites, marked with filled blue circles in Fig. 9A, the records took the form of simple slow potentials (Fig. 9B). In 14 of these 15 sites, the recording location was in a non-contracting area of the velum. Two sites, marked with filled red circles in Fig. 9A, were located mid-way between the two sets of Claus' fibres and records from these sites (Fig. 9C) had overshooting action potentials with a distinct undershoot. At another 15 sites, marked with filled black circles in Fig. 9A, there was a composite response consisting of a spike-like event arising from the top of a slow potential (Fig. 9D,E). All 15 of these composite responses were obtained from contracting regions of the velum.

Fig. 9B shows two records from a tight cluster of four recording sites. The stimulating electrode was at a different location for each recording. The associated chart (Fig. 9A, bottom right) identifies the stimulating sites outside the velum for the two selected records. The stimulus location for the thicker trace is indicated by a filled blue circle and that for the thinner trace by an open circle in Fig. 9A. The overall shape of the voltage response remained the same for all four sets of records but the response time depended on how far away the stimulus electrode had been placed. There was a linear relationship between the time from the stimulus to slow potential onset and the distance between stimulating and recording sites. The slope of the line (20 cm s^{-1}; R^2=0.97; temperature 10°C) suggested that excitation travelled from the stimulus site at a fixed rate and entered the velum in the vicinity of the recording pipette.

The question arises as to whether slow potentials represent electrotonic current spreading from the exumbrella epithelium, perhaps through gap junctions (model 1; Fig. 9F). What kind of potential change might be generated by such a mechanism? Intracellular records from the hydromedusa *Euphysa japonica* (Josephson and Schwab, 1979) and extracellular records from *Nanomia* (G. O. Mackie and R.W.M, unpublished) show 10 ms duration epithelial impulses. Theoretical considerations (see Materials and Methods) mean that the records in Fig. 9C could represent electrotonic spread from the neighbouring exumbrella. If so, the slow potentials recorded at other sites might be far enough away from this source for them to represent the slow rise and fall of a two-dimensional current spread (Jack et al., 1975). However, this remote current source would be inconsistent with our previous conclusion that the source of the slow potentials in Fig. 9B is in the vicinity of the recording site.

Another possibility is that the slow potentials are synaptic potentials generated by a nerve input to the Claus' fibres (model 2; Fig. 9F). To test this, we examined the total delay associated with the spread of excitation from the stimulating electrode to the muscle. This total delay is equivalent to the impulse initiation delay at the stimulating electrode plus the time for epithelial conduction, plus any delay in the process of transmission between epithelium and muscle. Extrapolating the delay at different stimulus sites to zero distance eliminates the epithelial conduction time.

Journal of Experimental Biology (2020) 223, jeb233494. doi:10.1242/jeb.233494

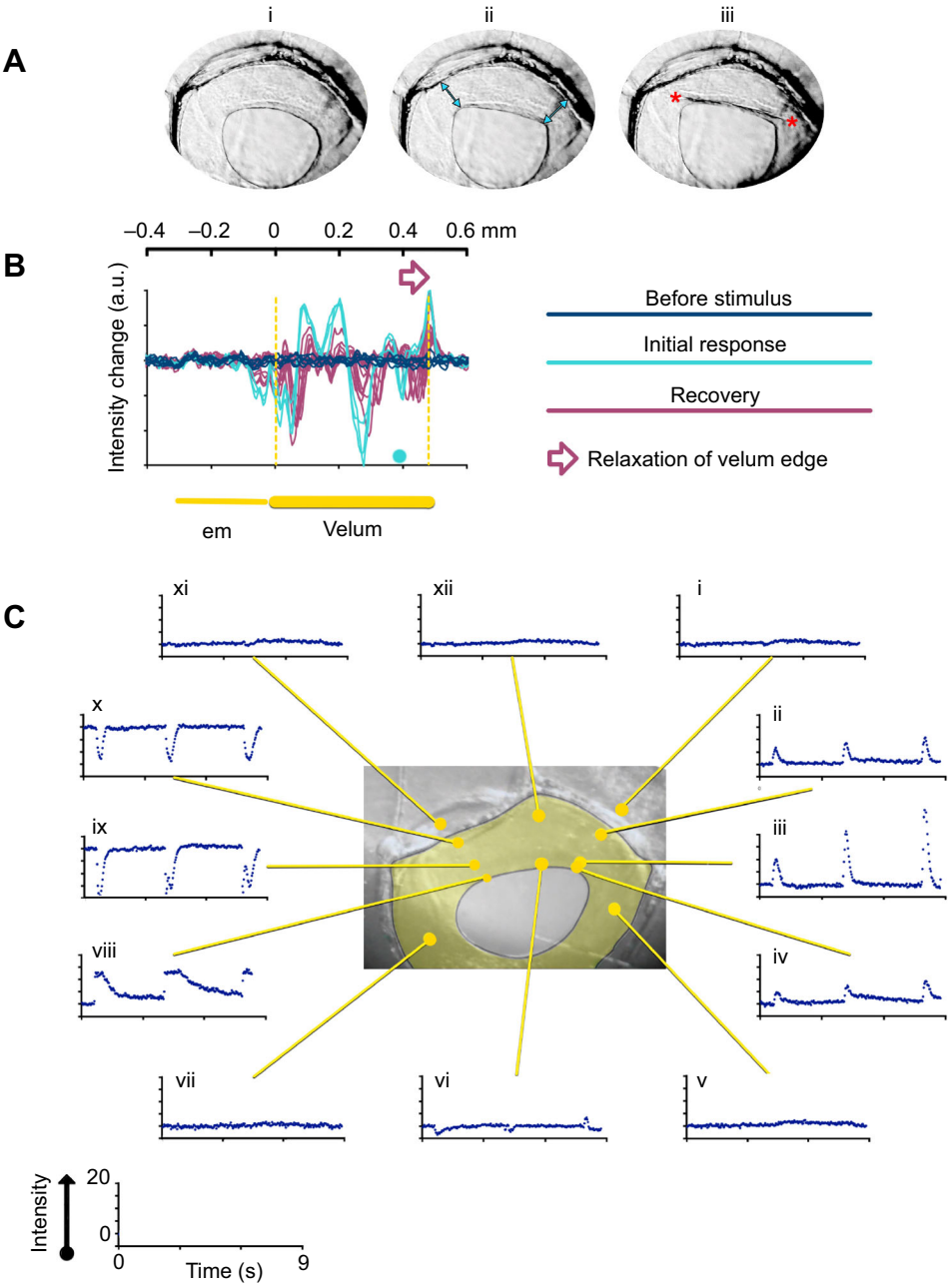

Fig. 8. Velum movement with epithelial stimulation. (A) Images collected at 30 frames s^{-1} before (i) and after (ii, iii) epithelial stimulation. The stimulating electrode on the exumbrella epithelium was 1.4 mm from the velum margin, at 60 deg from the vertical on the left hand side. Arrows in Aii indicate the position of Claus' fibres. Red stars in Aiii are at either end of a fold in the velum. (B) Changes in transmitted light intensity measured pixel by pixel as described in Materials and Methods. Dark blue line, baseline changes before the stimulus; light blue line, change from baseline for the three frames immediately after the stimulus; purple line, change from baseline during recovery. The nectophore bell margin is at 0 mm. Velum position before epithelial stimulation is shown by the yellow dashed lines; distal edge after stimulation is indicated by the filled light blue circle. Open arrow shows the lateral movement of the velum during recovery. em, endodermal muscle fibres; a.u., arbitrary units. (C) Changes in light intensity associated with three suprathreshold stimuli; average values at selected areas on the velum surface identified by the central chart. A–C are three different isolated nectophores bathed in seawater with 20 mmol l^{-1} Tris-HCl pH 7.6; temperature, 13°C.

Isolated nectophores were bisected between the two sets of Claus' fibres along the upper and lower nerve tracts. In these experiments, the recording site remained constant while the stimulation point ranged widely over the exumbrella epithelium. Fig. 10A shows a schematic representation of a divided-nectophore preparation, traced from stored images. The velum is in yellow and the black spots show the location of the cactus spines used to stabilize the half-preparation and flatten it as much as possible. The recording site (open red circle in Fig. 10A) is located on the velum just outside of the light-sensitive pigmented region (Totton, 1954; Mackie, 1962). The open blue circles in Fig. 10A represent eight different stimulation sites. The typical extracellular record obtained is shown in Fig. 10B (blue trace). The delay between the onset of the stimulus and the initial rise of the response (green arrowhead in Fig. 10B) is plotted in Fig. 10C (blue circles) against the distance between stimulus and recording sites. The data points were fitted by a straight line with a slope showing that the signal travelled with a conduction velocity of 35.7 cm s^{-1}. Extrapolation to the y-axis showed that the fixed component to the delay was 1.4 ms. The regression line R^2 value is 0.98.

A similarly high R^2 value (0.96) was obtained when fitting data from a second experiment (red symbols in Fig. 10C). In this case, there were 12 different stimulation sites and the velum response was more spike like (red trace in Fig. 10B). The conduction velocity was 24.7 cm s^{-1} and the fixed delay was 1.4 ms. Spike-like responses were recorded from three other experiments when the suction pipette was placed at the border between the pigmented area and the Claus' fibre region. One preparation consisted of an intact nectophore; in the other two, the nectophore had been bisected, either as in Fig. 10 or at right angles. A similar relationship between conduction time and conduction distance was obtained in each case. The mean (±s.e.m.) value for the conduction velocity was 30±

Journal of Experimental Biology

Journal of Experimental Biology (2020) 223, jeb233494. doi:10.1242/jeb.233494

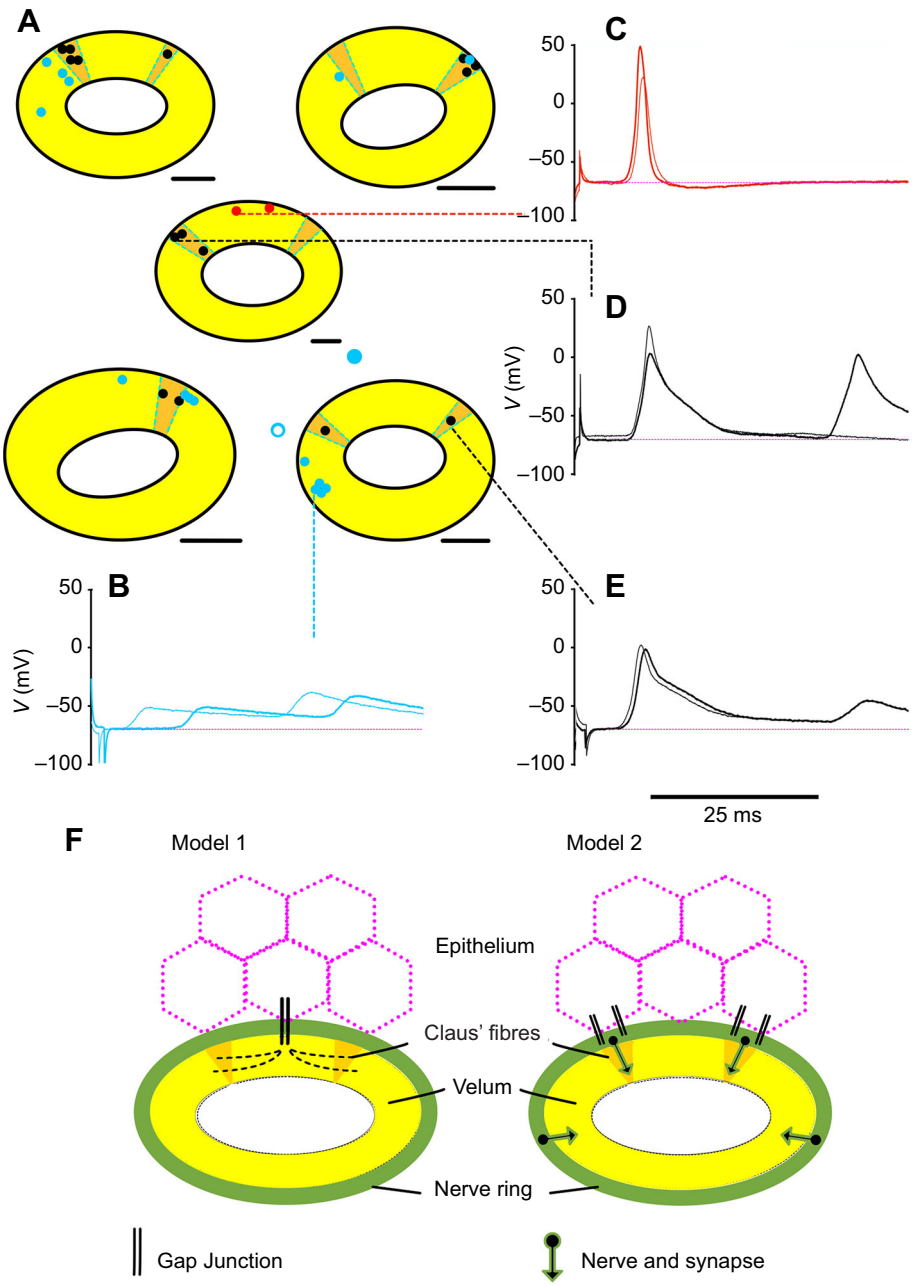

Fig. 9. Intracellular recordings from identified regions of velum. (A) Chart of recording sites traced from five different preparations; the velum is shown in yellow. The more darkly shaded regions indicate the extent of the visible contraction upon epithelial stimulation. (B–E) Typical intracellular recordings from selected sites; thicker lines are from the site indicated by the dashed line; thinner lines are from neighbouring sites. Recording sites within the velum are colour coded; blue, sites with slow events (B); red, sites with undershooting action potentials (C); black, sites with composite potentials (D,E). In B, records were obtained using different stimulating sites on the exumbrella epithelium. The furthest site (filled blue circle) produced the thicker trace; the nearer site (open blue circle) produced the thinner trace. The time scale refers to all records. (F) Models to account for excitation of the velum. In model 1, current spreads via gap junctions in the sub-delta region. In model 2, there are gap junctions between the epithelium and the nerve ring, and synaptic junctions between the nerve ring and the velum. All preparations were in seawater plus 10 mmol l^{-1} Tris buffer at pH 7.6; temperature, 10–13°C.

1.9 cm s^{-1} (n=5) and for the delay it was 1.3±0.09 ms (n=5). The temperature range for these experiments was 11.5–15°C. A trial using a recording site mid-way between the sets of Claus' fibres and halfway across the velum was unsuccessful because the delay was variable even at a fixed stimulating site. Here, the spike waveform was preceded by a slow rise to threshold (3 ms ramp) and may be caused by a variable input from multiple remote sites.

Suction electrodes were used to record propagating signals from the exumbrella surface itself (G. O. Mackie, personal communication). Three electrodes (one stimulating and two recording) were arranged in a straight line on the surface of an isolated nectophore. When the distance between the recording electrodes was 2.1 mm, the time taken to travel between them was 7.5 and 8 ms in two separate trials (experiment identifier: 52117). Thus the conduction velocity was 26–28 cm s^{-1}, in line with the values reported here. The mean fixed delay of 1.3 ms is greater than the value of 0.7 ms (at 12°C) obtained for the synaptic delay found in *A. digitale* (Kerfoot et al., 1985) but the mean delay at the stimulating electrode could be as much as 0.6 ms.

DISCUSSION

The degree of neuronal complexity reported here makes it unlikely that the *N. bijuga* colony relies on its nectophores simply for locomotion. The major network, the nerve ring, is associated with two lateral complexes as well as projections from them. There is also a 'ganglionic' nerve cell cluster in the delta region of the upper nerve tract and, at the stem attachment point, a 'terminal group' of cell bodies associated with the lower nerve tract. Added to this, the nectophore's exumbrella epithelium acts as an adjunct to the nervous system during backward swimming (Mackie, 1964). Below, we describe the neuroanatomy of other structures that may be concerned with subsidiary nectophore functions before discussing the link that translates epithelial signals into Claus' muscle excitation and the contribution of endodermal muscles to backwards swimming.

Journal of Experimental Biology (2020) 223, jeb233494. doi:10.1242/jeb.233494

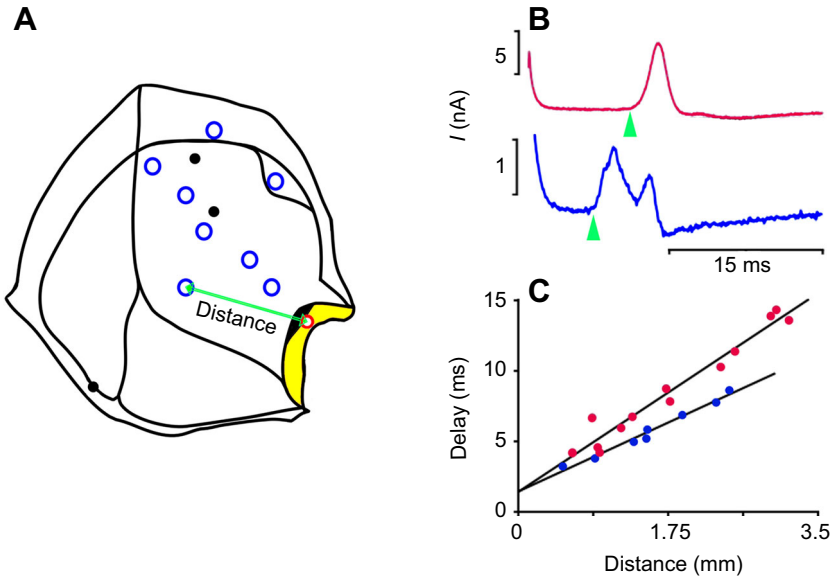

Fig. 10. Signal conduction from exumbrella epithelium to the velum. (A) Schematic representation of a half-nectophore preparation pinned flat with cactus spines (filled black circles). The extracellular recording site (open red circle) is located on the surface of the velum (yellow) just outside of the black-pigmented area. The open blue circles show the different positions of the bipolar stimulating electrode. (B) Extracellular recordings of velar muscle responses to electrical stimulation of the exumbrella epithelium (two different preparations). The response delay is defined as the time from the onset of the stimulus to the initial rise of the response (arrowhead). (C) Delay of the response plotted against the distance between the stimulating electrode and the recording site (green arrow in A). Blue data points correspond to stimulation sites shown in A with a typical extracellular recording being shown in B (blue); red data points are from a second preparation with the typical extracellular recording shown in red in B. The best fit was provided by regression analysis. Both preparations were bathed in seawater plus 25 mmol l^{-1} Tris buffer at pH 7.6 (plus 20% isotonic $MgCl_2$; red data points only); temperature, 13–15°C. Suction pipette tip diameter, 10–15 μm.

Nematocytes

Although elements of the upper nerve tract overlap individual nematocytes on the prominent nectophore ridges (Fig. 6), they may not make synaptic contact. Similar structures in the siphonophore *Cordalgama cordiformis* are without nerve connections and are thought to be purely defensive (Carré and Carré, 1980). In *N. bijuga*, their defensive role may be to entangle debris, preventing it from getting between nectophore bells or from entering them during the refilling process.

Flask-like structures

The flask-like structures at the bell margin have a good supply of nerves. Many have a large opening (Fig. 5) and appear to have released their contents. We have no evidence as to their function except to say that their location would be ideal for releasing secretions into the surrounding water during each swim.

Stem contact point

Under duress, the *N. bijuga* colony releases one or more of its nectophores. Once released, the nectophore undergoes a protracted sequence of spontaneous swims, which may serve to distract predators (Mackie et al., 1987). The contact point between nectophore and stem is the autotomy site, seen in isolated nectophores as a pronounced 'scar'. On the nectophore side, a large muscular pedicel houses an endodermal canal, which is a point of origin for the nectophore's four radial canals (Mackie, 1964). Next to the scar is a ganglionic structure (Fig. 2), made up of the cell bodies of the lower tract axons. In *Hippopodius*, another siphonophore, this is where nervous activity in the stem translates into epithelial impulses in the nectophore and vice versa (Bassot et al., 1978).

Exumbrella nerve processes

These fine nerve processes, many arising from elongated cell bodies, thread their way between flat epithelial cells while spreading around the upper and back surfaces of each nectophore. They converge on the mid-line and give rise to the upper nerve tract, which enters the nerve ring near its central point. Shorter processes enter the ring at points away from the central trunk. They are discrete units rather than a dense interconnecting network (Fig. 3) confirming Mackie's (1964) Methylene Blue study. The function of the upper nerve tract is unknown although a sensory role seems likely.

Lower nerve tract

This is necessary for forward swimming (Mackie, 1964), but whether elements in the tract synapse with elements in the outer nerve ring or whether they are continuous is not clear (Fig. 2B). In either case, excitation must pass from the tract to the outer nerve ring and from there to the inner nerve ring and on to the swimming myoepithelium. Electron micrographs show neurites passing through holes in the mesogloea between the inner and outer nerve rings (Jha and Mackie, 1967), but the subumbrella contains no nerve plexus such as might conduct excitation through the swimming muscles. A reasonable conclusion (Mackie, 1960) is that the impulses are conducted through the striated muscle sheet itself.

Endodermal muscles

Concerted action involving endodermal and exodermal muscles is unusual but does contribute to defensive behaviour in other hydrozoans (Mackie, 1986). Defensive involution in *Hippopodius* depends on contracting ectodermal fibres causing the velum to curl outward while contracting endodermal fibres make the pseudovelum roll inward, carrying the curled velum with it (Bassot et al., 1978). Endodermal muscles also contribute to the unusual form of defensive crumpling seen in the limnomedusan *Probosidactyla flavicirrata* (Spencer, 1975).

During reverse swimming in *N. bijuga*, the ectodermal Claus' fibres in the velum and the endodermal muscles that abut them at the margin contract together. The Claus' fibres shorten but only their distal ends move inwards; there is little distortion at the bell margin (Fig. 8B). This absence of movement suggests that the ectodermal and endodermal muscle groups generate equal and opposite forces, the endodermal fibres performing a fixator function. At the margin, movement is constrained by the isometric contraction of the endodermal fibres, which are anchored to the mesogloea at their distal ends and meet the Claus' fibres proximally. It is because the Claus' fibres are less constrained at their distal ends that the velum changes its shape so as to deflect the swimming thrust forwards.

Exumbrella epithelium

A natural stimulus for backward swimming is when anterior parts of the colony strike some resistant object. An electrical shock anywhere on the exumbrella surface reproduces the effect by initiating a conducted impulse in the surface epithelium (Mackie,

1964). This leads to Claus' fibre contraction, but the site of translation from epithelium to muscle is not known. It is likely to be near the nerve ring because the time taken for excitation to travel to the velum matches the conduction velocity of the epithelial impulses. Intracellular recordings (Fig. 9) place constraints on models of this process and suggest two possibilities. In model 1, there is an electrotonic input to the velum in the sub-delta region immediately below the margin. Because of the way current spreads in thin epithelia, an action potential in the epithelium would appear as a brief depolarizing event in the Claus' fibres (as in Fig. 9C). Slow potentials would represent the spread of current from this source. Another possibility is that the slow potentials represent a synaptic input to the Claus' fibres themselves, the epithelial impulse having entered the nervous system at some site in the nerve ring (model 2). The large fixed delay measured in Fig. 10 would tend to support this idea, but both models are not without difficulties.

The difficulty with model 1 is that the sub-delta area does not immediately contract in response to an epithelial stimulus. In model 2, the absence of movement might be explained by the matching tension produced by earlier contractions of the Claus' fibres on either side. However, why is there no spread of slow potentials into the sub-delta region? One possibility is that current spreads further along the muscle fibres than it does between them (as in *Aglantha digitale*; Kerfoot et al., 1985). If so, it is necessary to account for the slow potentials in Fig. 9B (and the reduction in delay with local stimulation) by assuming that the synaptic input is extensively distributed.

In other species, there are neural links between effectors and conducting epithelia. In the larvacean *Oikopleura labradoriensis*, tactile stimulation elicits escape, and the skin epithelium is connected by gap junctions to axons known to initiate locomotion (Bone and Mackie, 1975). In hydromedusae such as *Polyorchis*, the protective 'crumpling' that follows stimulation of the exumbrella epithelium only occurs if the radial muscles responsible make synaptic contact with neurites in the outer nerve ring (King and Spencer, 1981). In the siphonophore *Hippopodius*, stimulation of the exumbrella produces a similar defence response (Bassot et al., 1978). Electron microscopy fails to reveal any synapses or nerves (Bassot et al., 1978), but the response is associated with the inhibition of endogenous swimming, which is hard to explain with a purely electrical model. See Meech (2017) for references to other interactions between epithelia and nerves.

In *N. bijuga*, a conclusive answer awaits a quantitative analysis of current flow in the velum. Nevertheless, it seems that in other species there is a neural step between epithelia and muscle, and our estimate of the 'synaptic delay' in *N. bijuga* would support this explanation. Although synaptic inputs appear to be distributed around the bell margin, an especially important location is likely to be at the junction between the endodermal and Claus' fibres because the nerve ring deviates sharply here, plunging downward to meet them. It seems probable that the endodermal fibres have a neural input at this point.

Acknowledgements
We thank the Director and Staff of Friday Harbor Labs, University of Washington, USA, without whose support this work could not have been completed. We also thank Claudia Mills for her support and endless encouragement. We are indebted to George Mackie for initiating this work and allowing us to include his measurements of epithelial conduction velocity. His insights have been invaluable and one of us in particular (R.W.M.) has benefited from his patient explanations of siphonophore anatomy. We also thank three anonymous referees for their carefully considered comments and suggestions.

Competing interests
The authors declare no competing or financial interests.

Author contributions
Conceptualization: T.P.N., R.W.M.; Methodology: T.P.N., R.W.M.; Validation: T.P.N., R.W.M.; Formal analysis: T.P.N., R.W.M.; Investigation: T.P.N., R.W.M.; Resources: T.P.N., R.W.M.; Data curation: T.P.N., R.W.M.; Writing - original draft: T.P.N., R.W.M.; Writing - review & editing: T.P.N., R.W.M.; Visualization: T.P.N., R.W.M.; Funding acquisition: T.P.N., R.W.M.

Funding
T.P.N. was supported by National Science Foundation (NSF) grants 1548121, 1557923 and 1645219, and by Human Frontier Science Program grant RGP0060/2017 to Leonid Moroz. R.W.M. was supported in part by Natural Sciences and Engineering Research Council of Canada grant OGP0001427 01 to George Mackie.

Supplementary information
Supplementary information available online at
https://jeb.biologists.org/lookup/doi/10.1242/jeb.233494.supplemental

References
Bassot, J.-M., Bilbaut, A., Mackie, G. O., Passano, L. M. and Pavans De Ceccatty, M. (1978). Bioluminescence and other responses spread by epithelial conduction in the siphonophore *Hippopodius*. *Biol. Bull.* **155**, 473-498. doi:10.2307/1540785

Bone, Q. and Mackie, G. O. (1975). Skin impulses and locomotion in *Oikopleura* (Tunicata: Larvacea). *Biol. Bull.* **149**, 267-286. doi:10.2307/1540527

Carré, D. and Carré, C. (1980). On triggering and control of cnidocyst discharge. *Mar. Behaviour. Physiol.* **7**, 109-117. doi:10.1080/10236248009386975

Church, S. H., Siebert, S., Bhattacharyya, P. and Dunn, C. W. (2015). The histology of *Nanomia bijuga* (Hydrozoa: Siphonophora). *J. Exp. Zool. B Mol. Dev. Evol.* **324**, 435-449. doi:10.1002/jez.b.22629

Claus, C. (1878). Uber *Halistemma tergestinum* n. sp. nebst bemerkungen fiber den feineren bau der Physophoriden. *Arb. Zool. Inst. Univ. Wien.* **1**, 1-56.

Costello, J. H., Colin, S. P., Gemmell, B. J., Dabiri, J. O. and Sutherland, K. R. (2015). Multi-jet propulsion organized by clonal development in a colonial siphonophore. *Nat. Commun.* **6**, 8158. doi:10.1038/ncomms9158

Gladfelter, W. B. (1972). Structure and function of the locomotory system of *Polyorchis montereyensis* (Cnidaria, Hydrozoa). *Helgolander wiss. Meeresunters.* **23**, 38-79. doi:10.1007/BF01616310

Grimmelikhuijzen, C. J. P., Spencer, A. N. and Carré, D. (1986). Organization of the nervous system of physonectid siphonophores. *Cell. Tissue Res.* **246**, 463-479. doi:10.1007/BF00215186

Haddock, S. H. D., Dunn, C. W. and Pugh, P. R. (2005). A re-examination of siphonophore terminology and morphology, applied to the description of two new prayine species with remarkable bio-optical properties. *J. Mar. Biol. Assoc. UK* **85**, 695-707. doi:10.1017/S0025315405011616

Jack, J. J. B., Noble D. and Tsien, R. W. (1975). Electric current flow in excitable cells. Clarendon Press, Oxford.

Josephson, R. K. and Schwab, W. E. (1979). Electrical properties of an excitable epithelium. *J. gen. Physiol.* **74**, 213-236. doi:10.1085/jgp.74.2.213

Jacobs, W. (1962). Floaters of the sea. *Nat. Hist.* **71**, 22-27. doi:10.1038/nbt0104-27

Jha, R. K. and Mackie, G. O. (1967). The recognition, distribution and ultrastructure of Hydrozoan nerve elements. *J. Morph.* **123**, 43-61. doi:10.1002/jmor.1051230105

Kerfoot, P. A. H., Mackie, G. O., Meech, R. W., Roberts, A. and Singla, C. L. (1985). Neuromuscular transmission in the jellyfish *Aglantha digitale*. *J. Exp. Biol.* **116**, 1-25.

King, M. G. and Spencer, A. N. (1981). The involvement of nerves in the epithelial control of crumpling behaviour in a Hydrozoan jellyfish. *J. Exp. Biol.* **94**, 203-218.

Mackie, G. O. (1960). The structure of the nervous system in *Velella*. *Quart. J. Microscopical Sci.* **101**, 119-131.

Mackie, G. O. (1962). Pigment effector cells in a cnidarian. *Science.* **137**, 689-690. doi:10.1126/science.137.3531.689

Mackie, G. O. (1964). Analysis of locomotion in a siphonophore colony. *Proc. R. Soc. B Biol. Sci.* **159**, 366-391. doi:10.1098/rspb.1964.0008

Mackie, G. O. (1986). From aggregates to integrates: physiological aspects of modularity in colonial animals. *Phil. Trans. Roy. Soc. B Biol. Sci.* **313**, 175-196. doi:10.1098/rstb.1986.0032

Mackie, G. O., Pugh, P. R. and Purcell, J. E. (1987). Siphonophore biology. *Adv. Mar. Biol.* **24**, 97-262. doi:10.1016/S0065-2881(08)60074-7

Mariscal, R. N. (1974). Nematocysts. In *Coelenterate Biology* (ed. L. Muscatine and H. M. Lenhoff), pp. 129-178. New York: Academic Press.

Meech, R. W. (2017). The evolution of neurons. In *The Wiley Handbook of Evolutionary Neuroscience* (ed. S. V. Shepherd), pp. 88-124. Chichester, UK: John Wiley and Sons Ltd.

Norekian, T. P. and Moroz, L. L. (2016). Development of neuromuscular organization in the Ctenophore *Pleurobrachia bachei*. *J. Comp. Neurol.* **524**, 136-151. doi:10.1002/cne.23830

Norekian, T. P. and Moroz, L. L. (2019a). Neuromuscular organization of the Ctenophore *Pleurobrachia bachei*. *J. Comp. Neurol.* **527**, 406-436. doi:10.1002/cne.24546

Norekian, T. P. and Moroz, L. L. (2019b). Neural system and receptor diversity in the ctenophore *Beroe abyssicola*. *J. Comp. Neurol.* **527**, 1986-2008. doi:10.1002/cne.24633

Norekian, T. P. and Moroz, L. L. (2020a). Comparative neuroanatomy of ctenophores: neural and muscular systems in *Euplokamis dunlapae* and related species. *J. Comp. Neurol.* **528**: 481-501. doi:10.1002/cne.24770

Norekian, T. P. and Moroz, L. L. (2020b). Atlas of the neuromuscular system in the Trachymedusa *Aglantha digitale*: Insights from the advanced hydrozoan. *J. Comp. Neurol.* **528**:1231-1254. doi:10.1002/cne.24821

Östman, C. (2000). A guideline to nematocyst nomenclature and classification, and some notes on the systematic value of nematocysts. *Sci. Mar.* **64**, 31-46. doi:10.3989/scimar.2000.64s131

Roberts, W. M. and Almers, W. (1992). Patch voltage clamping with low-resistance seals: loose patch clamp. *Methods Enzymol.* **207**, 155-176. doi:10.1016/0076-6879(92)07011-C

Satterlie, R. A. and Spencer, A. N. (1983). Neuronal control of locomotion in hydrozoan medusae. *J. Comp. Physiol.* **150**, 195-206. doi:10.1007/BF00606369

Spencer, A. N. (1975). Behavior and electrical activity in the hydrozoan *Proboscidactyla flavicirrata* (Brandt). II. The Medusa. *Biol. Bull.* **149**, 236-250. doi:10.2307/1540493

Totton, A. K. (1954). Siphonophores of the Indian Ocean. *Discovery Repts.* **27**, 1-162.

Wehland, J. and Willingham, M. C. (1983). A rat monoclonal antibody reacting specifically with the tyrosylated form of alpha-tubulin. II. Effects on cell movement, organization of microtubules, and intermediate filaments, and arrangement of Golgi elements. *J. Cell Biol.* **97**, 1476-1490. doi:10.1083/jcb.97.5.1476

Wehland, J., Willingham, M. C. and Sandoval, I. V. (1983). A rat monoclonal antibody reacting specifically with the tyrosylated form of alpha-tubulin. I. Biochemical characterization, effects on microtubule polymerization *in vitro*, and microtubule polymerization and organization *in vivo*. *J. Cell Biol.* **97**, 1467-1475. doi:10.1083/jcb.97.5.1467

Weill, R. (1934). *Contribution à l'étude des cnidaires et de leurs nématocystes. I: Recherces sur les Nematocystes (Morphologie, Physiologie, Developpement), II: Valeur Taxonomique du Cnidome*. Paris: Les Presses Universitaires de France.